26

Robot assisted 3D shape acquisition by optical systems

Cesare Rossi, Vincenzo Niola, Sergio Savino and Salvatore Strano
University of Naples "Federico II"
ITALY

1. Introduction

In this chapter, a short description of the basic concepts about optical methods for the acquisition of three-dimensional shapes is first presented. Then two applications of the surface reconstruction are presented: the passive technique Shape from Silhouettes and the active technique Laser Triangolation. With both these techniques the sensors (telecameras and laser beam) were moved and oriented by means of a robot arm. In fact, for complex objects, it is important that the measuring device can move along arbitrary paths and make its measurements from suitable directions. This chapter shows how a standard industrial robot with a laser profile scanner can be used to achieve the desired d-o-f.
Finally some experimental results of shape acquisition by means of the Laser Triangolation technique are reported.

2. Methods for the acquisition of three-dimensional shapes

In this paragraph the computational techniques are described to estimate the geometric property (the structure) of the three-dimensional world (3D), starting from ist bidimensional projections (2D): the images. The shape acquisition problem (shape/model acquisition, image-based modeling, 3D photography) is introduced and all steps that are necessary to obtain true tridimensional models of the objects, are synthetized [1].
Many methods for the automatic acquisition of the shape object exist. One possible classification of the methods for shape acquisition is illustrated in figure 1.
In this chapter optical methods will be analyze. The principal advantages of this kind of techniques are the absence of contact, the rapidity and the economization. The limitations include the possibility of being able to acquire only the visible part of the surfaces and the sensibility to the property of the surfaces like transparency, brilliance and color.
The problem of image-based modeling or 3D photography, can be described in this way: the objects irradiate visible light; the camera capture this "light", whose characteristics depend on the lighting system of the scene, surface geometry, reflecting surface; the computer elaborates the light by means of opportune algorithms to reconstruct the 3D structure of the objects.

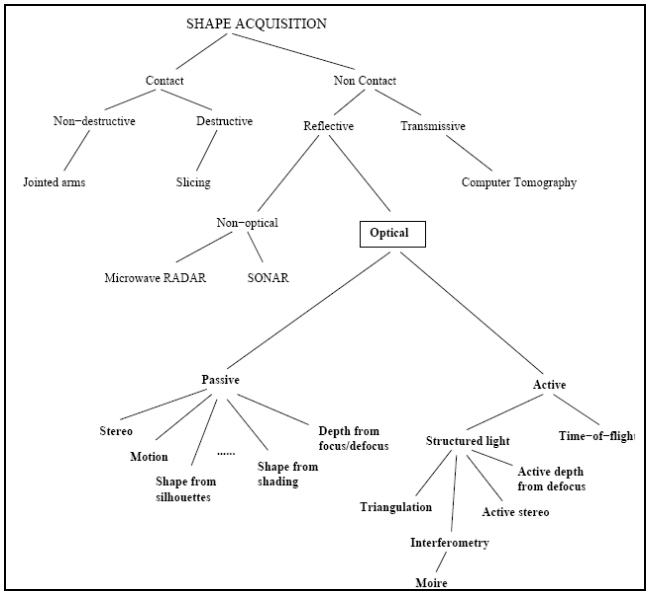

Fig. 1. Classification of the methods for shape acquisition [1]

In the figure 2 is shown an equipment for the shape acquisition by means two images.

Fig. 2. Stereo acquisition

The fundamental distinction between the optical techniques for shape acquisition, regards the use of special lighting sources. In particular, it is possible to distinguish two kinds of optical methods: active methods, that modify the images of scene by means of opportune luminous pattern, laser lights, infrared radiations, etc., and passive methods, that analyze the images of the scene without to modify it. The active methods have the advantage to concur high resolutions, but they are more expensive and not always applicable. The passive methods are economic, they have fewer constraints obligatory, but they are characterized by lower resolutions.

Many of the optical methods for the shape acquisition have like result an image range, that is an image in which every pixel contains the distance from the sensor, of a visible point of the scene, instead of its brightness (figure 3). An image range is constituted by measures

(discrete) of a 3D surface respect to a 2D plan (usual the plane image sensor) and therefore it is also called: 2.5D image. The surface can be always expressed in the form Z = f(X, Y), if the reference plane is XY. A sensor range is a device that produces an image range.

Fig. 3. Brightness reconstruction of an image [1]

Below optical sensor range is any optical system of shape acquisition, active or passive, that is composed of equipment and softwares and that gives back an image range of the scene.
The main characteristics of a sensor range are:

- **resolution**: the smallest change of depth that the sensor can find;
- **accuracy**: diffrence between measured value (average of repeated measures) and true value (it measures the systematic error);
- **precision**: statistic variation (standard deviation) of repeated measures of a same quantity (dispersion of the measures around the average);
- **velocity**: number of measures in a second.

2.2 From the measure to the 3D model

The recovery of 3D information, however, does not exhaust the process of shape acquisition, even if it is the fundamental step. In order to obtain a complete model of an object, or of a scene, many images range are necessary, and they che they must be aligned and merged with each other to obtain a 3D surface (like poligonal mesh).
The reconstruction of the model of the object starting from images range, previews three steps:

- **adjustment**: (or alignment) in order to transform the measures supplied from the several images range in a one common reference system;
- **geometric fusion**: in order to obtain a single 3D surface (typically a poligonal mesh) starting various image range;
- **mesh simplification**: the points given back by a sensor range are too many to have a manageable model and the mesh must be simplified.

Below the first phase will be described above all, the second will be summarily and the third will be omitted.
An image range Z(X,Y) defines a set of 3D points (X,Y,Z(X,Y)), figure 4a. In order to obtain a surface in the 3D space (surface range) it is sufficient connect between their nearest points with triangular surfaces (figure 4b).

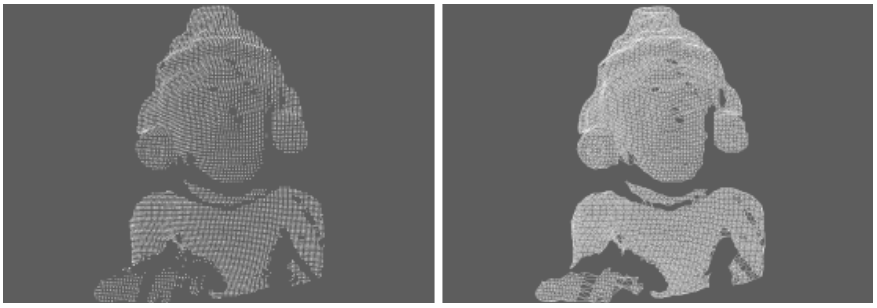

a) b)

Fig. 4. Image range result (a) and its surface range (b) [1].

In many cases depth discontinuities can not be covered with triangles in order to avoid making assumptions that are unjustified on the shape of the surface. For this reason it is desirable to eliminate triangles with sides too long and those with excessively acute angles.

2.3 Adjustment

The sensors range don't capture the shape of an object with a single image, many images are needed, each of which captures a part of the object surface. The portions of the surface of the object are obtained by different images range, and each of them is made in its own reference system (that depends on sensor position).
The aim of adjustment is to expres all images in the same reference system, by means of an opportune rigid transformation (rotation and translation).
If the position and orientation of the sensor are known, the problem is resolved banally. However in many cases, the sensor position in the space is unknown and the transformations can be calculated using only images data, by means of opportune algorithms, one of these is ICP (Iterated Closest Point).
In the figure 5, on the left, eight images range of an object are shown, each in its own reference system; on the right, all images are were superimposed with adjustment operation.

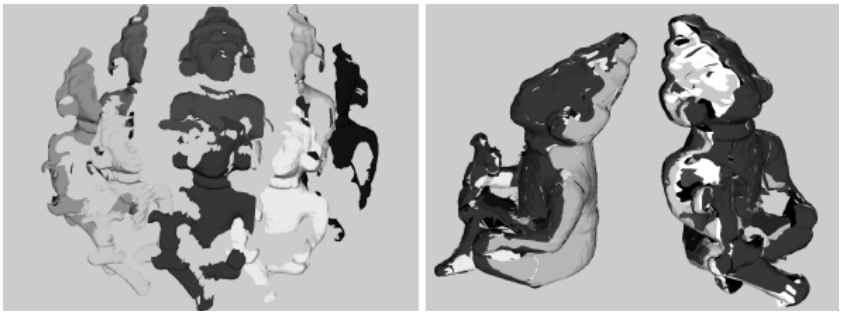

Fig. 5. Images range and result of adjustment operation [1]

2.4 Geometric fusion

After all images range data are adjusted in one reference system, they be united in a single shape, represented, as an example, by triangular mesh. This problem of surface reconstruction, can be formulated like an estimation of the bidimensional variety which approximates the surface of the unknown object by starting to a set of 3D points. The methods of geometric fusion can be divided in two categories:

- **Integration of meshes**: the triangular meshes of the single surfaces range, are joined.
- **Volumetric fusion**: all data are joined in a volumetric representation, from which a triangular mesh is extracted.

2.4.1 Integration of meshes

The techniques of integration of meshes aim to merge several 3D overlapped triangular meshes into a single triangular mesh (using the representation in terms of surface range).
The method of Turk and Levoy (1994) merges overlapped triangular meshes by means of a technique named "zippering". The overlapping meshes are eroded to eliminate the overlap and then it is possible to use a 2D triangolation to sew up the edges. To make this the points of the two 3D surface close to edges, must be projected onto a plane 2D.
In the figure 6, on the left, two aligned surface are shown, and on the right, the zippering result is shown.

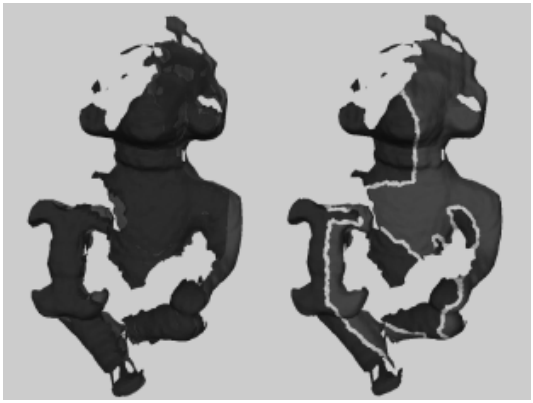

Fig. 6. Aligned surface and zippering result

The techniques of integration of meshes allow the fusion of several images range without losing accuracy, since the vertices of the final mesh coincide with the points of the measured data. But, for the same reason, the results of these techniques are sensitive to erroneous measurements, that may cause problems in the surface reconstruction.

2.4.2 Volumetric Fusion

The volumetric fusion of surface measurements constructs an intermediate implicit surface that combines the measurements overlaid in a single representation. The implicit

representation of the surface is an iso-surface of a scalar field f(x,y,z). As an example, if the function of field is defined as the distance of the nearest point on the surface of the object, then the implicit surface is represented by f(x,y,z) = 0. This representation allows modeling of the shape of unknown objects with arbitrary topology and geometry.
To switch from implicit representation of the surface to a triangular mesh, it is possible to use the algorithm Marching Cubes, developed by Lorensen e Cline (1987) for the triangulation of iso-surfaces from the discrete representation of a scalar field (as the 3D images in the medical field). The same algorithm is useful for obtaining a triangulated surface from volumetric reconstructions of the scene (shape from silhouette and photo consistency).
The method of Hoppe and others (1992) neglects the structure of the data (surface range) and calculates a surface from the unstructured "cloud" of points.
Curless and Levoy (1996) instead, take advantage of the information contained in the images range in order to assign the voxel that lie along the sight line that, starting from a point of the surface range, arrives to the sensor.
An obvious limitation of all geometric fusion algorithms based on an intermediate structure of discrete volumetric data is a reduction of accuracy, resulting in the loss of details of the surface. Moreover the space required for the volumetric representation grows quickly when resolution grows.

2.5 Optical methods for the shapes acquisition

All computational techniques use some indications in order to calculate the shape of the objects starting from the images. Below the main methods divided between active and passive, are listed.

Passive optical methods:

- depth from focus/defocus
- shape from texture
- shape from shading
- stereo-photometric
- stereopsis
- shape from silhouette
- shape from photo-consistency
- structure from motion

Active optical methods:

- active defocus
- active stereo
- active triangolation
- interferometry
- flight time

All the active methods, except the last one, employ one or two cameras and a source of special light, and fall in the wider class of the methods with **structured lighting system**.

3. Three-dimensional reconstruction with technique: Shape from Silhouettes

In this paragraph one of the passive optical techniques of 3D reconstruction will be introduced in detail, with some obtained results.

3.1 Principle of volumetric reconstruction from shapes

The aim of volumetric reconstruction is to create a representation that describes not only the surface of a region, but also the space that it encloses. The hypothesis is that there is a known and limited volume, in which the objects of interest lie. A 3D box is modelled to be an initial volume model that contains the object. This box is divided in discrete elements called voxels, that are three-dimensional equivalent of bidimensional pixel. The reconstruction coincides with the assignment of a label of occupation (or color) to each element of volume. The label of occupation is usually binary (transparent or opaque).
Volumetric reconstruction offers some advantages compared to traditional stereopsi techniques: it avoids the difficult problem of finding correspondences, it allows the explicit handling of occlusions and it allows to obtain directly a three-dimensional model of the object (it is not necessary to align parts of the model) integrating simultaneously all sights (which are the order of magnitude of ten).
Like in the stereopsi, the cameras are calibrated.
Below one of the many algorithms developed for the volumetric reconstruction from silhouettes of an object of interest is described: shape from silhouettes .
Shape From Silhouettes is well-known technique for estimating 3D shape from its multiple 2D images.
Intuitively the silhouette is the profile of an object, comprehensive of its inside part. In the "Shape from Silhouette" technique silhouette is defined like a binary image, which value in a certain point (x, y) underlines if the optical ray that passes for the pixel (x, y) intersects or not the object surface in the scene. In this way, Every point of the silhouette, respectively of value "1" or "0", identifies an optical ray that intersects or not the object.
To store the labels of the voxel it is possible to use the octree data structure.The octree are trees with eight ways in which each node represents a part of space and the children nodes represents the eight divisions of that part of space (octants).

3.1.1 Szeliski algorithm

The Szeliski algorithm allows to build the volumetric model by means of octree structure.
The octree structure is constructed subdividing each cube in eight part (octants), starting from the root node that represents the initial volume. Each cube has associated a color:

- black: it represents a occupied volume;
- white: it represents an empty volume;
- gray: it represents an inner node whose classification is still uncertain.

For each octant, it is necessary to verify if its projection in image i, is entire contained in the black region. If that happens for all N shapes, the octant is labeled as black. If instead, the octant projection is entire contained in the background (white), also for a single camera, the octant is labeled as white. If one of these two cases happens, the octant becomes a leaf of the octree and it is not more tried, otherwise, it is labeled as gray and it is subdivided in eight parts. In order to limit the dimension of the tree, gray octants with minimal dimension, are

labeled as black. At the end of process it is possible to obtain an octree that represents 3D object structure.
An example of volumetric model construction with Szeliski algorithm is shown in figure 7.

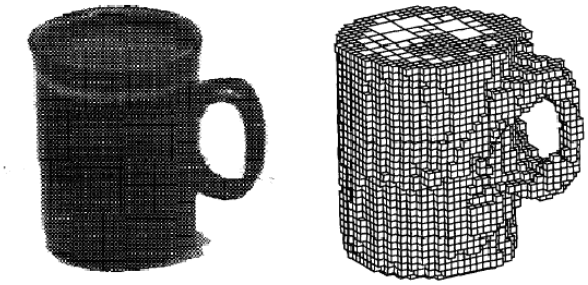

Fig. 7. Model reconstruction with Szeliski algorithm

3.1.2 Proposed method

The analysis method is to define a voxel box that contains the object in three dimensional space and to discard subsequently those points of the initial volume that have an empty intersection with at least one of the cones of the shapes obtained from the acquired images.
The voxel will have only binary values, black or white.
The algorithm is performed by projecting the center of each voxel into each image plane, by means of the known intrinsic and extrinsic camera parameters. If the projected point is not contained in the silhouette region, the voxel is removed from the object volume model.

3.2 Images elaboration

Starting from an RGB image (figure 8), it is analized and, by means of segmentation procedure, it is possible to obtain object silhouette reconstruction.

Fig. 8. RGB image

Segmentation is the process by means of which the image is subdivided in characteristics of interest. This operation is based on strong intensity discontinuities or regions that introduce homogenous intensity on the base of established criteria. There are four kinds of discontinuities: points, lines, edge, or, in a generalized manner, interest points.

In order to separate an object from the image background, the method of the threshold s is used: each point (u,v) with f(u,v) > s (f(u,v) < s) is identified like object, otherwise like background. The described elaboration is used to identify and characterize the various regions that are present in each image; in particular, by means of this technique it is possible to separate the objects from the background.
The first step is to transform RGB image in gray scale image (figure 9), in thi way the intensity value becomes a threshold to identify the object in the image.

Fig. 9. Gray scale image

The gray scale image is a matrix, whose dimensions correspond to number of pixel along the two directions of the sensor, and whose elements have values in range [0,255]. Subsequently, a limited set of pixel that contains the projection of the object in the image plane, is selected, so it is possible to facilitate the segmentation procedure (figure 10).

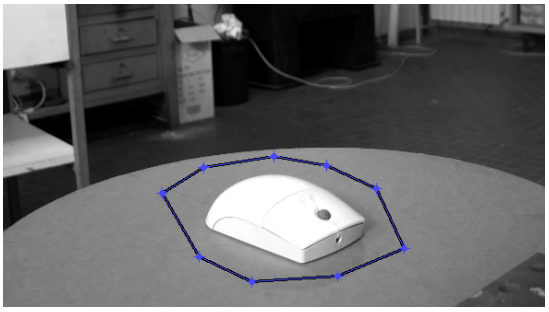

Fig. 10. Object identification

In gray scale image, pixel with intensity f(u,v) different from that of points that are not representative of object (background T), are chosen. This tecnique is very effective, if in the image there is a real difference between object and background.
For each pixel (u, v) unit value or zero, respectively, is assigned, if it is an optical beam passing through the object or not (figure 11).

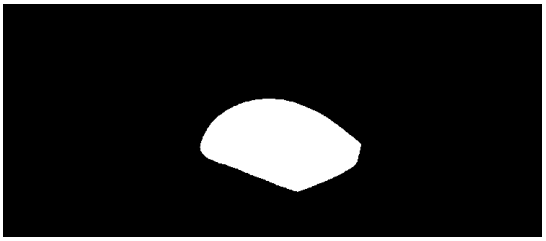

Fig. 11. The computed object silhouette region

3.3 Camera calibration

It is necessary to identify all model parameters in order to obtain a good 3-D reconstruction. Calibration is a basic procedure for the data analysis.
There are many kind of procedure to calibrate a camera system, but in this paragraph the study of the calibration procedures will not be discussed in detail.
The aim of calibration procedure is to obtain all intrinsic and estrinsic parameters of the camera system. Calibration procedure is based on a set of images, taken with a target placed in different positions that are known in a base reference system. A least square optimization allows to identify all parameters.

3.4 The proposed algorithm

The result of image elaboration is the object silhouette region for each image with pixel coordinates and centroid coordinates of these region in image reference system, (Fig. 11).
By means of calibration parameters (intrinsic and estrinsic), it is possible to evaluate, for each image, an homogeneous transformation matrix, between the image reference system of each image and a base reference system.
The first step is to discretize a portion of work space by mean an opportune box divided in voxels (figure 12). In this operation, it is necessary to choose the number of voxels, the dimension of box and its position in a base reference system. The position of voxel is chosen evaluating the intersections in base reference system, of the camera optical axis that pass through silhouette centroids of at least, two images. Subsequently it is possible to divide the initial volume model in a number of voxels according to the established precision, and it is possible to evaluate the centers of voxels in base reference.

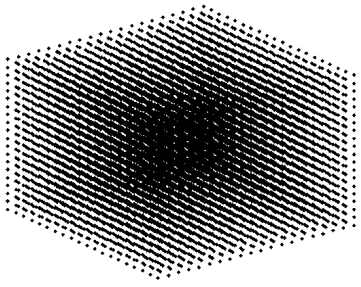

Fig. 12. Voxel discretization of workspace.

For each of the silhouettes, the projection of the centre of the voxels in the image plane can be obtained as follows:

$$\{\tilde{\phi}\}_j = [M]_i \cdot \{\tilde{w}\}_j \qquad i = 1,...,p \qquad j = 1,...,q \tag{1}$$

Where p is the number of silhouettes, q is the number of the voxels and $[M]_i$ is the transformation matrix between the base frame and the image frame.
The algorithm is performed by projecting the center of each voxel into each image plane, by means of the known intrinsic and extrinsic camera parameters. If the projected point is not contained in the silhouette region, the voxel is removed from the object volume model. This yields the following relation:

$$\begin{Bmatrix} u \\ v \\ 0 \\ 1 \end{Bmatrix}_j = [\tilde{\phi}]_j = [M]_p \cdot \{\tilde{w}\}_j \qquad j = 1,...,q \qquad 1 \le u \le n \qquad 1 \le v \le m \tag{2}$$

Where n and m are the number of pixels along the directions u and v, respectively. So a matrix [A] having dimension [n,m] is written; the values of the elements of this matrix is one if corresponds to a couple of coordinates (u,v) obtained by eq. (2) that belongs to the object silhouette in the image; otherwise the value is zero:

$$[A] := a_{hk} = 1 \qquad h = u_j, k = v_j \tag{3}$$

A set of pixels having coordinates $(\overline{u}, \overline{v})$, belonging to the first silhouette, is defined as follows:

$$\Omega_1 := (\overline{u}, \overline{v})_1 \tag{4}$$

The points of the image that belong to the silhouette are defined as follows:

$$I_1(u,v) = \begin{cases} 1 & (u,v) \subseteq \Omega_1 \\ 0 & (u,v) \not\subset \Omega_1 \end{cases} \qquad 1 \le u \le n \qquad 1 \le v \le m \tag{5}$$

By the product among the matrix defined in eq. (3) with the matrix in eq. (5), the following set of indexes is obtained:

$$\bar{j} : [A] \cdot [I_1] = 1 \qquad 1 \le u \le n \qquad 1 \le v \le m \tag{6}$$

Now the points (in the base frame) which indexes are integer numbers belonging to the set $\bar{j}$ are considered. These points are used as starting points to repeat the same operations,

described by eq. (2), for all the other images. This procedure is recursive and is called space carving technique.

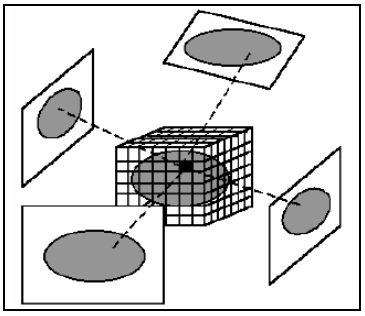

Fig. 13. Scheme of space carving technique.

3.5 Evaluation of the resolution

The choosen number of voxels defines the resolution of the reconstructed object.
Consider a volume which dimensions are l_x, l_y and l_z and a discretization along the three directions: Δ_x, Δ_y e Δ_z, the object resolutions that can be obtained in the three directions are:

$$a_x = \frac{l_x}{\Delta_x}; a_y = \frac{l_y}{\Delta_y}; a_z = \frac{l_z}{\Delta_z} \tag{7}$$

In figure 14 two examples of reconstruction with different resolution choices are shown.

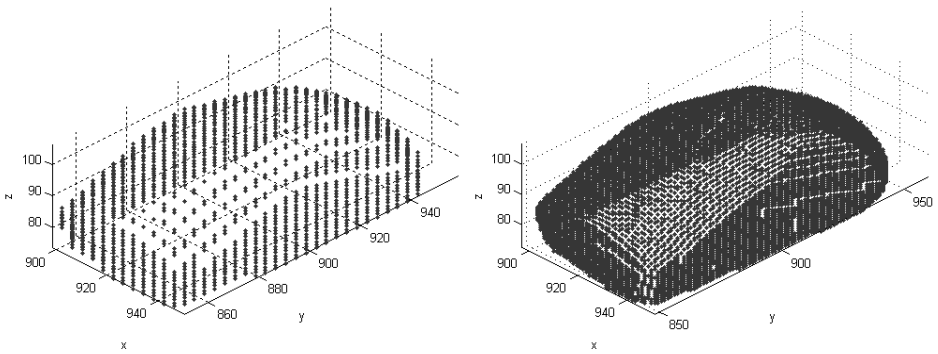

Fig. 14. Examples of reconstructions with different resolutions.

It must be pointed out that the choice of the initial box (resolution) depends on the optical sensor adopted. It is clear that an object near to the sensor will appear bigger than a far one, hence the error achieved for the same unit of discretization is increased with the distance for a given focal length.

$$a^c_u = \delta_u \cdot \frac{w_\varsigma}{f}; a^c_v = \delta_v \cdot \frac{w_\varsigma}{f} \quad (8)$$

Obviously it must be checked that the choosen initial resolution is not bigger than the resolution that the optical sensor can achieve. To this pourpose, once the object has been reconstructed, the minimum dimension that can be recorded by the camera is computed by eq. (8); the latter is compared with the resolution initially stated.
This techique is rater slow because it is necessary to project each voxel of the initial box in the image plane of each of the photos. Moreover, a big number of phots is required and the procedure can not be made in real –time. It must also be noted, however, that this procedure can be used in a rater simple way in order to obtain a rough evaluation of the volume and of the shape of an object.
This techinque is very suitable to be assisted by a robot arm. Infact the accuracy of the reconstruction obtained depends on the number of images used, on the positions of each viewpoint considered, on the camera's calibration quality and on the complexity of the object shape. By positioning the camera on the robot, it is possible to know, exactly, not only the characteristics of the camera, but also the position of the camera reference frame in the robot work space. Therefore the camera intrinsic and extrinsic parameters are known without a vision system calibration and it's easy to make an elevated number of photos. That is to say, it could be possible to obtain vision system calibration, robot arm mechanical calibration and trajectories recording and planning.

4. Three-dimensional reconstruction by means of Laser Triangolation

The laser triangulation technique maily permits higher operating speed with a satisfacting quality of reconstruction.

4.1 Principle of laser triangolation

In this paragraph is described a method for surface reconstruction, that uses of a linear laser emitter and a webcam, and uses triangulation principle applied to a scanning belt on object surface.
Camera observes the intersection between laser and object: laser line points in image frame, are the intersections between image plane and optical rays that pass through the intersection points between laser and object. By means of a transformation matrix, it is possible to express the image frame coordinates, in pixel, in a local reference frame. In figure 15 a) is shown a scheme of scanning system: {W} is local reference frame, {I} is image frame with coordinates system {u,v}, and {L} is laser frame. {L2} is laser plane that contains laser knife and scanning belt on the surface of object, and it coincides with (x,y) plane of laser frame {L}. Starting from the coordinates in pixel (u,v), in image frame, it is possible to write the coordinates of the scanning belt on the object surface, in camera frame by means of equation (9). Camera frame is located in camera focal point figure 15 b).

$$\begin{Bmatrix} x_c \\ y_c \\ z_c \\ 1 \end{Bmatrix} = \begin{bmatrix} \delta_x & 0 & 0 & -\delta_x u_0 \\ 0 & \delta_y & 0 & -\delta_y v_0 \\ 0 & 0 & 0 & f \\ 0 & 0 & 0 & 1 \end{bmatrix} = \begin{Bmatrix} u \\ v \\ 0 \\ 1 \end{Bmatrix} \tag{9}$$

with:
(u_0,v_0): image frame coordinates of focal point projection in image plane;
(δ_x, δ_y): physical dimension of sensor pixel along direction u and v;
f: focal length.

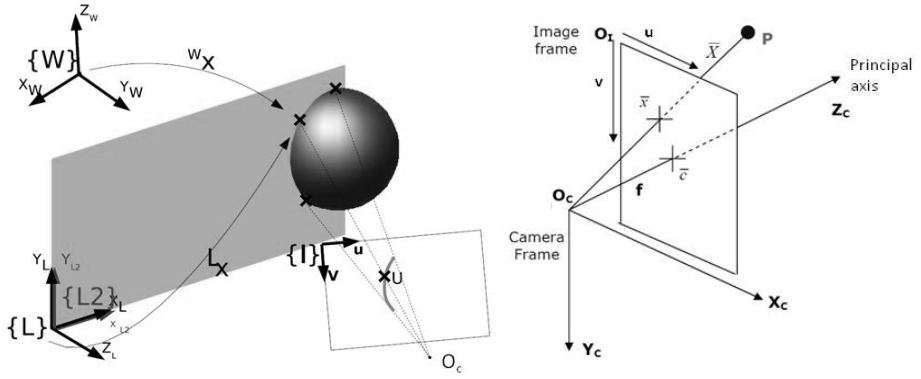

a) b)

Fig. 15. Scheme of scanning system

It is possible to write the expression of the optical beam of a generic point in the image frame, that can be identified by means of parameter t.

$$\begin{cases} x_c = (u - u_0)\delta_u t \\ y_c = (v - v_0)\delta_v t \\ z_c = ft \end{cases} \tag{10}$$

Laser frame {L} is rotated and translated respect to camera frame, the steps and their sequence are:
Translation Δx_{lc} along axis x_c;
Translation Δy_{lc} along axis y_c;
Translation Δz_{lc} along axis z_c;
Rotation φ_{lc} around axis z_c;
Rotation θ_{lc} around axis y_c;
Rotation ψ_{lc} around axis x_c ;
Hence in equation (11) the transformation matrix between laser frame and camera frame is:

$$\left[{}^{c}T_{l}\right]=\begin{bmatrix}1&0&0&0\\0&\cos(\psi_{lc})&-\sin(\psi_{lc})&0\\0&\sin(\psi_{lc})&\cos(\psi_{lc})&0\\0&0&0&1\end{bmatrix}\cdot\begin{bmatrix}\cos(\theta_{lc})&0&\sin(\theta_{lc})&0\\0&1&0&0\\-\sin(\theta_{lc})&0&\cos(\theta_{lc})&0\\0&0&0&1\end{bmatrix}\cdot$$
$$\begin{bmatrix}\cos(\varphi_{lc})&-\sin(\varphi_{lc})&0&0\\\sin(\varphi_{lc})&\cos(\varphi_{lc})&0&0\\0&0&1&0\\0&0&0&1\end{bmatrix}\cdot\begin{bmatrix}1&0&0&0\\0&1&0&0\\0&0&1&\Delta z_{lc}\\0&0&0&1\end{bmatrix}\cdot\begin{bmatrix}1&0&0&0\\0&1&0&\Delta y_{lc}\\0&0&1&0\\0&0&0&1\end{bmatrix}\cdot\begin{bmatrix}1&0&0&\Delta x_{lc}\\0&1&0&0\\0&0&1&0\\0&0&0&1\end{bmatrix} \quad (11)$$

Laser plane {L2} coincides with (x,y) plane of laser frame {L}, so it contains three points:

$$\{p\}_{l}=\{0,0,0,1\}^{T};\{q\}_{l}=\{1,0,0,1\}^{T};\{r\}_{l}=\{0,0,1,1\}^{T} \quad (12)$$

In camera frame:

$$\{p_x,p_y,p_z,1\}_{c}^{T}=\left[{}^{c}T_{l}\right]^{-1}\{p\}_{l};\{q_x,q_y,q_z,1\}_{c}^{T}=$$
$$\left[{}^{c}T_{l}\right]^{-1}\{q\}_{l};\{r_x,r_y,r_z,1\}_{c}^{T}=\left[{}^{c}T_{l}\right]^{-1}\{r\}_{l} \quad (13)$$

It is possible to obtain laser plane equation in camera frame, solving equation (14) in xc, yc and zc.

$$\det\begin{bmatrix}x_c-p_x&y_c-p_y&z_c-p_z\\q_x-p_x&q_y-p_y&q_z-p_z\\r_x-p_x&r_y-p_y&r_z-p_z\end{bmatrix}=0 \quad (14)$$

If it is:

$$M_x=\det\begin{bmatrix}q_y-p_y&q_z-p_z\\r_y-p_y&r_z-p_z\end{bmatrix};M_y=\det\begin{bmatrix}q_x-p_x&q_z-p_z\\r_x-p_x&r_z-p_z\end{bmatrix};$$
$$M_z=\det\begin{bmatrix}q_x-p_x&q_y-p_y\\r_x-p_x&r_y-p_y\end{bmatrix}$$

equation in camera frame, is:

$$(x_c-p_x)M_x-(y_c-p_y)M_y+(z_c-p_z)M_z=0 \quad (15)$$

It is possible to evaluate coordinates xc, yc e zc, in camera frame, solving system (16) with unknown t:

$$\begin{cases} x_c = (u - u_0)\delta_x t \\ y_c = (v - v_0)\delta_y t \\ z_c = ft \\ (x_c - p_x)M_x - (y_c - p_y)M_y + (z_c - p_z)M_z = 0 \end{cases} \tag{16}$$

The solution is:

$$t = \frac{p_x M_x - p_y M_y + p_z M_z}{(u - u_o)\delta_x M_x - (v - v_o)\delta_y M_y + fM_z} \tag{17}$$

Equation (17) permits to compute in the camera frame, the points coordinates of the scanning belt on the object surfaces, starting to its image coordinates (u,v). In this way it is possible to carry out a 3-D objects reconstruction by means of a laser knife.

4.2 Detection of the laser path

A very important step for 3-D reconstruction is image elaboration for the laser path on the target, [5, 6, 7] , the latter is shown in figure 16.

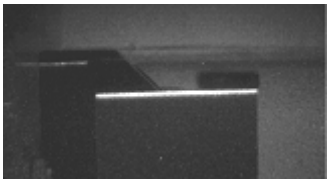

Fig.16. Laser path image.

Image elaboration procedure permits to user to choose some image points of laser line, in order to identify three principal colours (Red, Green, and Blue) of laser line, figure 17.

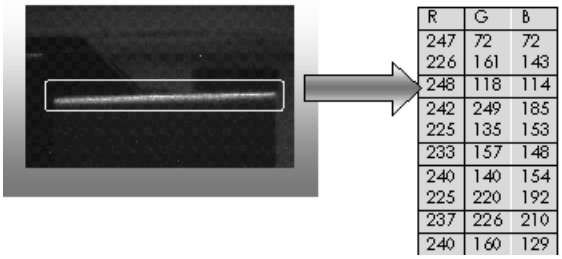

R	G	B
247	72	72
226	161	143
248	118	114
242	249	185
225	135	153
233	157	148
240	140	154
225	220	192
237	226	210
240	160	129

Fig. 17. Image matrix representation.

With mean values of scanning belt principal colours, it is possible to define a brightness coefficient of the laser line, according to relation (18):

$$s = \frac{\max(\text{mean}(R), \text{mean}(G), \text{mean}(B)) + \min(\text{mean}(R), \text{mean}(G), \text{mean}(B))}{2} \tag{18}$$

By means of relation (19), an intensity analysis is carried out on RGB image.

$$L(u,v) = \frac{\max(R,G,B) + \min(R,G,B)}{2} \tag{19}$$

By equation (19), the matrix that contains the three layers of RGB image, is transformed in a matrix L, that represents image intensity. This matrix represents same initial image, but it gives information only about luminous intensity in each image pixel, and so it is a grayscale expression of initial RGB image, figure 18 a) and b).

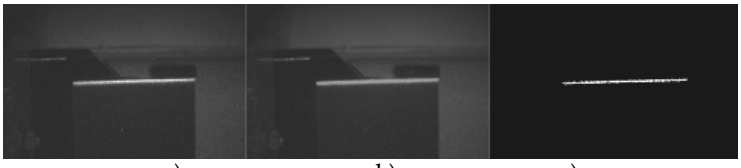

a) b) c)

Fig. 18. a)RGB initial image ; b)grayscale initial image L ; c) matrix Ib.

With relation (20), it is possible to define a logical matrix Ib. Matrix Ib indicates pixels of matrix L with a brightness in a range of 15% brightness coefficient s.

$$I_b(u,v) = \begin{cases} 1 & \text{se} \quad 0.85 \cdot s \le L(u,v) \le 1.15 \cdot s \\ 0 & \text{otherwise} \end{cases} \tag{20}$$

In figure 18 c), matrix Ib is shown.

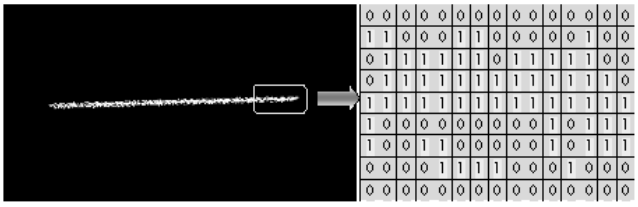

Fig. 19. I_b representation.

In matrix Ib, the scanning belt on the object surface (see fig. 19) is represented by means of the pixel value one. The area of the laser path in the image plane depends on the real dimension of laser beam and on external factors such as: reflection phenomena, inclination of object surfaces.

3-D reconstruction procedure is based on triangulation principle and it doesn't consider the laser beam thickness, so it is necessary to associate a line to the image of scanning belt.

Since the laser path in the image plane is rather horizontal, a geometrical mean is computed on, on the columns of the matrix Ib , that is to say: in the opposite direction to wider extension of the laser path in the image. This is shown in equation (21).

$$\Omega := \{u,v\}; \overline{\Omega} := \{\overline{u},\overline{v}\} \Rightarrow$$
$$\{\overline{u} = \frac{\sum_{u,v\in\Omega} uI_b(u,v)}{\sum_{u,v\in\Omega} I_b(u,v)} \neq \infty, \overline{v} = v : \sum_{u,v\in\Omega} I_b(u,v) \neq 0\} \tag{21}$$

Then a matrix hp is also defined as follows:

$$h_b(u,v) = \begin{cases} 1 & \text{se} \quad \{u,v\} \in \overline{\Omega} \\ 0 & \text{otherwise} \end{cases} \tag{22}$$

Matrix hb is hence a logical matrix with same dimension of Ib in which that represents laser image like a line, figure 20. This line is centre line of scanning belt on object surface in image.

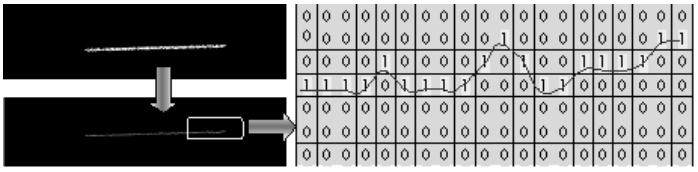

Fig. 20. h_b representation.

The set of transformations (19), (20) and (21) represents the image elaboration, that is necessary to identify a laser line in image. The points of this line are used in 3-D reconstruction procedure.

4.3 Calibration procedure

It is necessary to identify all model parameters in order to obtain a good 3-D reconstruction. Calibration is a basic procedure for the data analysis, [4, 6, 8]. For this reason, it was developed a calibration procedure for a classic laser scanner module.

The laser scanner module is composed by a web-cam with resolution 640x480 pixel and a linear laser. The calibration test rig is realized with a guide on which is fixed the laser scanner module and a digital micrometer with a target, figure 21 a).

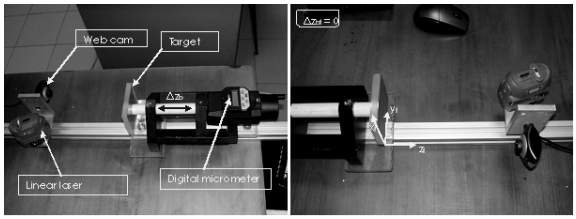

a) b)

Fig. 21. a) Laser scanner module calibration test rig; b) fixed frame $O_fx_fy_fz_f$.

A fixed frame $O_fx_fy_fz_f$ has origin in a vertex of the rectangular target with dimension a=68 mm and b=74.5 mm, like it is shown in figure 21 b). Target movements are indicated with Δzbf.
In figure 22 some steps of calibration procedure are shown.

Fig. 22. Calibration procedure steps.

Calibration procedure is based on a set of images, taken with the target placed in different positions respect to the laser scanner module. A least square optimization allows to identify all parameters. In figure 23 are shown 10 images used for calibration, of scanning belt, with 10 different Δzb_f.

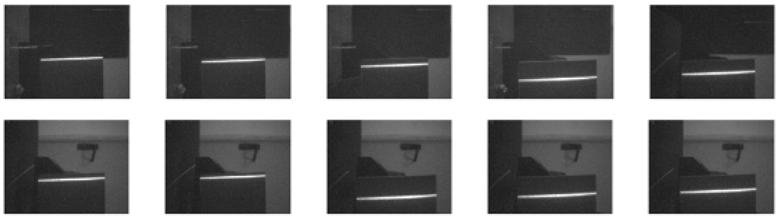

Fig. 23. Images used for calibration.

The aim of calibration procedure is to obtain the parameters that define the relation between laser frame LxLyLzL and camera frame $O_cx_cy_cz_c$, figure 15.
In every calibration step, it is possible to define transformation matrix between fixed frame $O_fx_fy_fz_f$ and target frame:

$$\left[{}^{f}T_{b}\right]_{i} = [1 \quad 0 \quad 0 \quad 0;0 \quad 1 \quad 0 \quad 0;0 \quad 0 \quad 1 \quad -\Delta z_{fb}^{i};0 \quad 0 \quad 0 \quad 1] \tag{23}$$

The transformation matrix between fixed frame $O_f x_f y_f z_f$ and camera frame $O_c x_c y_c z_c$ can be optained analogous to matrix $[^cT_l]$, and it is a function of six parameters:

$$\left[{}^{f}T_{c}\right] = f(\Delta x_{cf}, \Delta y_{cf}, \Delta z_{cf}, \psi_{cf}, \theta_{cf}, \varphi_{cf}) = f(\pi_{cf}) \tag{24}$$

with πcf set of parameter of transformation $[^fT_c]$.
Equation (11) can be written as:

$$\left[{}^{c}T_{l}\right] = g(\Delta x_{lc}, \Delta y_{lc}, \Delta z_{lc}, \psi_{lc}, \theta_{lc}, \varphi_{lc}) = f(\pi_{lc}) \tag{25}$$

with πlc set of parameter of transformation $[^cT_l]$.
For each step of the calibration procedure it is possible to evaluate the coordinates of the points of the laser line in the camera frame, according to equations (13) and (21):

$$\{\bar{x}_c, \bar{y}_c, \bar{z}_c, 1\}_i^T = f(\pi_{lc}, f) \cdot \{\bar{u}, \bar{v}, 0, 1\}_i^T \tag{26}$$

By means of equation (22), it is possible to write:

$$\begin{aligned} &\{\bar{x}_f, \bar{y}_f, \bar{z}_f, 1\}_i^T = \left[{}^{f}T_{c}\right]^{-1} \cdot \{\bar{x}_c, \bar{y}_c, \bar{z}_c, 1\}_i^T = \\ &\left[{}^{f}T_{c}\right]^{-1} \cdot f(\pi_{lc}, f) \cdot \{\bar{u}, \bar{v}, 0, 1\}_i^T = \omega(\pi_{cf}, \pi_{lc}, f) \cdot \{\bar{u}, \bar{v}, 0, 1\}_i^T \end{aligned} \tag{27}$$

The optimization problem can be defined as:

$$\min_{\rho \in R^{13}} F(\rho)^2 \tag{28}$$

F(ρ) is a vectorial function defined as:

$$\begin{aligned} F(\rho) = \{&(\bar{z}_f^{i+1} - \bar{z}_f^{i}) - (\Delta\bar{z}_{bf}^{i+1} - \Delta\bar{z}_{bf}^{i+1}), \min(\bar{x}_f^{i}), \\ &\max(\bar{x}_f^{i}) - a, \max(\bar{z}_f^{i}) - \min(\bar{z}_f^{i}), \\ &\max(\bar{y}_f^{i}) - \min(\bar{y}_f^{i}), \min(\bar{y}_f^{1}), \min(\bar{z}_f^{1})\}^T \end{aligned} \tag{29}$$

With a least square optimization, the unknown parameters of set [πcf, πlc, f] are identified.
An interactive GUI was developed to allow the user to acquire images, to execute optimization and to verify the results.
In figure 24, a graphical result of calibration is shown: it is possible to observe the camera frame position, the laser beam (represented by the quadrilateral on the left), and the 3-D reconstructions of scanning beam on target surface, for each image used in the calibration procedure.

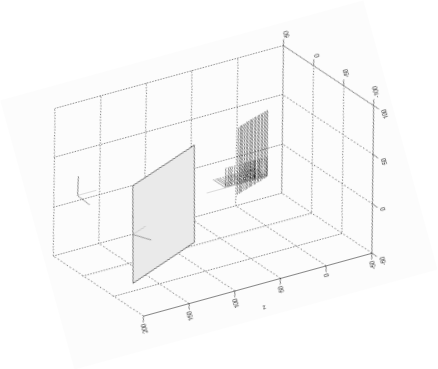

Fig. 24. Calibration results

4.4 System accuracy

4.4.1 Camera error

An obvious source of camera calibration error arises from the spatial quantization of the image. However, many times the image event of interest spans many pixels. It is then possible to calculate the centroid of this event to sub-pixel accuracy, thereby reducing the spatial quantization error. Limiting the sub-pixel accuracy is the fact that in general the perspective projection of an object's centroid does not equal the centroid of the object's perspective projection. However, often times the error incurred from assuming the centroid of the projection is the projection of the centroid is quite small [14].
Camera accuracy is a function of its distance from observed object.
If an unitary variation of pixels in the directions u and v is considered, from the equation (10) is gotten:

$$x_c = (u + 1 - u_0)\delta_x \frac{z_c}{f}$$
$$y_c = (v + 1 - v_0)\delta_y \frac{z_c}{f} \tag{30}$$

Calculating the difference respectively between x_c and y_c after and before the variation is gotten the accuracy of the system, that is the variation of x_c and y_c that it can be gotten for a minimum variation in terms of pixels in the image frame:

$$\Delta x_c = x_c(u + 1) - x_c(u)$$
$$\Delta y_c = y_c(v + 1) - y_c(v)$$

The image accuracies in directions x_c and y_c are:

$$a^c{}_x = \delta_u \cdot \frac{z_c}{f}$$

$$a^{c}{}_{y} = \delta_v \cdot \frac{z_c}{f} \tag{31}$$

4.4.2 Scanner module error

It is possible to define an accuracy expression for 3D-reconstruction that can be obtained by means of laser scanner module, according to equations (16) and (17).
A variation (α, β) of image coordinates (u,v), generates a variation of parameter t of equation (17):

$$\Delta t = \frac{-(p_x M_x - p_y M_y + p_z M_z)\cdot(\alpha\delta_x M_x - \beta\delta_y M_y)}{(u\delta_x M_x + \alpha\delta_x M_x - v\delta_y M_y - \beta\delta_y M_y + fM_z)\cdot(u\delta_x M_x - v\delta_y M_y + fM_z)} \tag{32}$$

where:
- α pixel variation in u direction;
- β pixel variation in v direction;

The variation of parameter t, allows to define an expression of accuracy of 3D reconstruction. In fact, by means of equation (16), it is possible to obtain the variation of coordinates in camera frame in function of variation of image coordinates:

$$\begin{cases} \Delta x_c = \alpha\delta_u \cdot \dfrac{p_x M_x - p_y M_y + p_z M_z}{(u - u_o + \alpha)\delta_x M_x - (v - v_o + \beta)\delta_y M_y + fM_z} + (u - u_0)\delta_x \cdot \Delta t \\ \Delta y_c = \beta\delta_v \cdot \dfrac{p_x M_x - p_y M_y + p_z M_z}{(u - u_o + \alpha)\delta_x M_x - (v - v_o + \beta)\delta_y M_y + fM_z} + (v - v_0)\delta_y \cdot \Delta t \\ \Delta z_c = \Delta t \cdot f \end{cases} \tag{33}$$

An unitary variation of image coordinates (α=1 and β=0, or α=0 and β=1, or α=1 and β=1), allows to define three accuracy parameters of scanner laser 3D reconstruction:

$$\begin{cases} a^{SL}{}_x = \Delta x_c \\ a^{SL}{}_y = \Delta y_c \\ a^{SL}{}_z = \Delta z_c \end{cases} \Rightarrow \text{with} \Rightarrow \begin{cases} (\alpha,\beta) = (0,1) \\ \text{or} \\ (\alpha,\beta) = (1,0) \\ \text{or} \\ (\alpha,\beta) = (1,1) \end{cases} \tag{34}$$

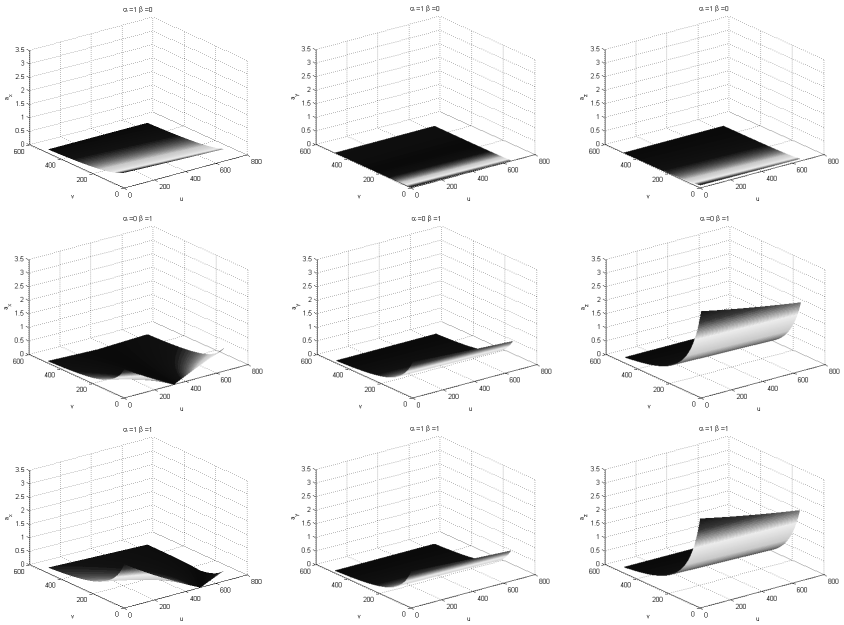

Fig. 25. Error of the accuracy

As it has shown in the figure 25, the worst accuracy of the laser scanner for a pixel variation is in the direction z_c. Besides it can be seen that az has minimum value for values of v = dv and it grows up to v = 1 with a non-linear law.

4.4.3 Laser precision

Most of the outlier and other erroneous points are caused by reflections. In these cases, the high energy laser beam is reflected from mirroring surfaces such as metal or glass. Therefore, too much light hits the sensor of the camera and so-called blooming effects occur. In other cases, a direct reflection may miss the camera. In addition, a part of the object may lie in the path from the projected laser line to the camera causing a shadowing effect. All these effects are responsible for gaps and holes. At sharp edges of some objects, partial reflections appear. In addition, craggy surfaces cause multiple reflections and, therefore, indefinite point correlations.

Furthermore, aliasing effects in the 2D image processing of laser beam, lead to high frequent noise in the generated 3D data [15].

The laser beam thickness in the image, can vary because of the above described effects, but 3-D reconstruction procedure is based on triangulation principle and it doesn't consider this phenomenon. In fact, the detection of laser path allows to identify a line in image with a thickness of a pixel.

The real laser beam thickness and its path thickness in the image, must be considered to evaluate the precision of 3D reconstruction.

The accuracy a^c_z becomes worse, if a thickness parameter is considered. This parameter is a generalized measure of laser beam thickness in pixel, and it can be expressed with two

components: thu thickness measure along direction u in image frame and thv thickness measure along direction v in image frame.
An expression of 3D reconstruction accuracy in direction z of camera frame, can be obtained by means of equation (11), in which parameters (α, β) are the generalized laser beam thickness (thu, thv):

$$\begin{cases} a_x = \Delta x_c \\ a_y = \Delta y_c \Rightarrow \text{with} \Rightarrow (\alpha,\beta) = (th_u/2, th_v/2) \\ a_z = \Delta z_c \end{cases} \tag{35}$$

The equations (32) define the resolution of the laser scanner 3-D reconstruction, and they allows to evaluate the accuracy of each point coordinates that is obtained with laser beam image elaboration.

4.5 Scanner range

Another characteristic of a 3D laser scanner is the minimum and the maximum distance between a generic point of a surface and the image plane. These parameters define the range of the scanning procedure. Decreasing the angle θ of inclination of the laser plane respect to the plane x_cz_c of the camera frame at a respective fixed distance s the range of scanning increases (figure 26).

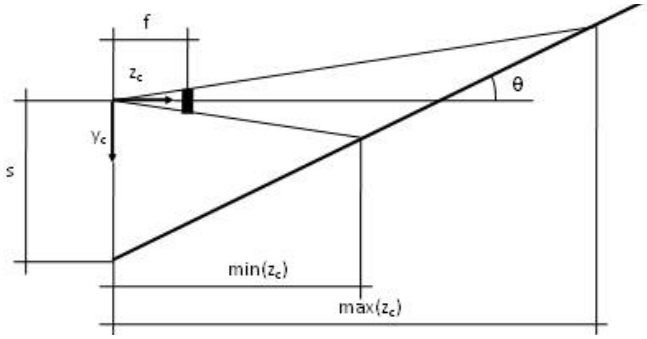

Fig. 26. The minimum and the maximum distance between a generic point of a surface and the image plane

This is not a good solution since to decrease of this angle the accuracy worsens notably as is shown in figure 27.

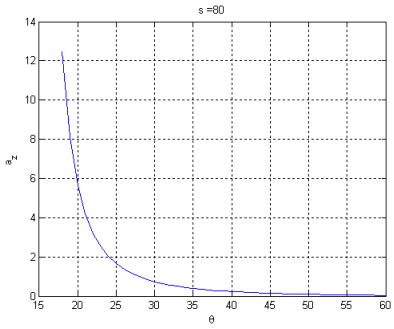

Fig. 27. Accuracy diagram.

For the considered system with values s = 90 mm and θ = 23° it have been gotten: max(zc) = 525 mm and min(zc) = 124 mm;

5. Experimental results

To evaluate the accuracy of the laser scanner system, the latter was fixed on a robot arm; in this way it was possible to capture a lot of shape information of the object from different views.

5.1 The test rig

5.1.1 Laser Scanner Module

Our rig, is based on a laser profile, that essentially consists in a line laser and a camera. The laser beam defines a "laser plane" and the part of the laser plane that lies in the image view of the camera is denoted the "scanning window", figure 28.

Fig. 28. Scanner module

The laser scanner device was realized by assembling a commercial linear laser and a common web-cam.

5.1.2 The Robot

In order to optimize the accuracy of the reconstruction resulting model, scanning should be adapted to the shape of the object. One way to do that is to use an industrial robot to move a laser profile scanner along curved paths.
The scanner laser module was mounted on a revolute robot with three d.o.f., designed and assembled in our Department, figure 29.

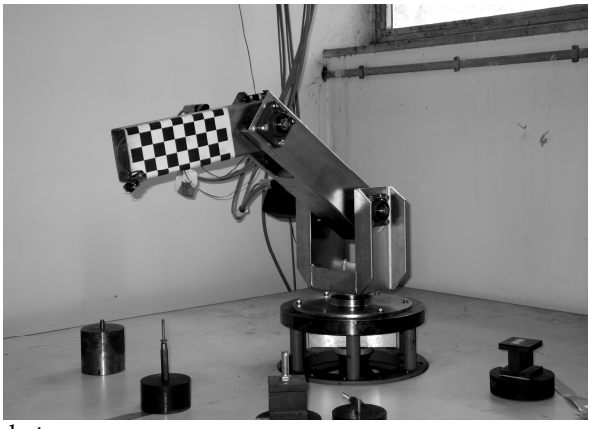

Fig. 29. Revolute robot

The robot serves as a measuring device to determine the scanning window position and orientation in 3D for each camera picture, with a great precision. All scan profiles captured during a scan sequence must be mapped to a common 3D coordinate system, and to do this, positional information from the robot were used [11]. Figure 30 shows the equipment at work.

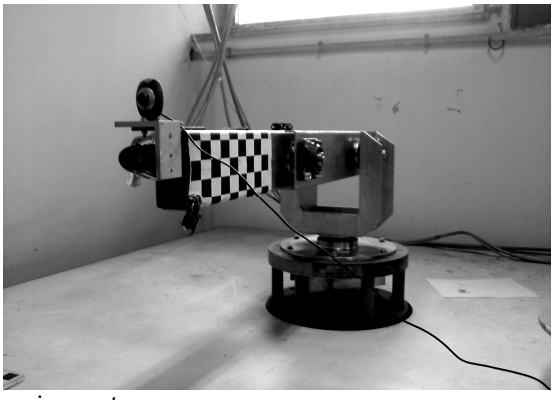

Fig. 30. The robot scanning system

The authors have developed a solution where the robot controller and scanner software work separately during a scan sequence that will be described in the following paragraphs.

5.2 The laser scanner on the robot model

When the laser scanner module is installed on the robot, figure 30, it is possible to use positional information from robot to determine the scanning window position and orientation in 3D.

Defining [DH] as the transformation matrix between coordinates in the robot base frame 0 (the fixed one) and those in frame 3 (the one of the last link), figure 31, for the coordinates of a generic point P exists this relationship:

$$\{P\}_0 = [DH] \cdot \{P\}_3 \tag{36}$$

The matrix [DH] depends on 9 constant kinematic structure parameters, that are known, and 3 variable joints position parameters that are measurable by means of robot control system.

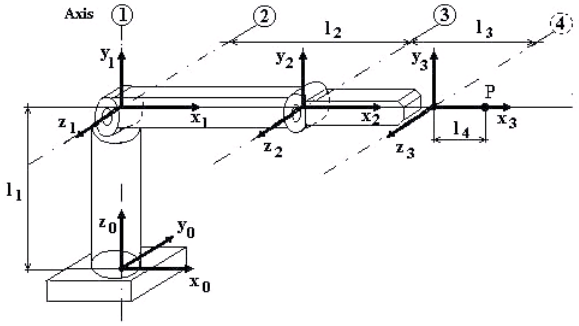

Fig. 31. Revolute robot scheme

Knowing the transformation matrix $[^cT_3]$ between the camera frame and the frame of the robot last link, it's possible to obtain a transformation matrix between the camera frame and the frame 0, figure 32.

$$\{P\}_c = [^cT_3] \cdot [DH]^{-1} \cdot \{P\}_0 \tag{37}$$

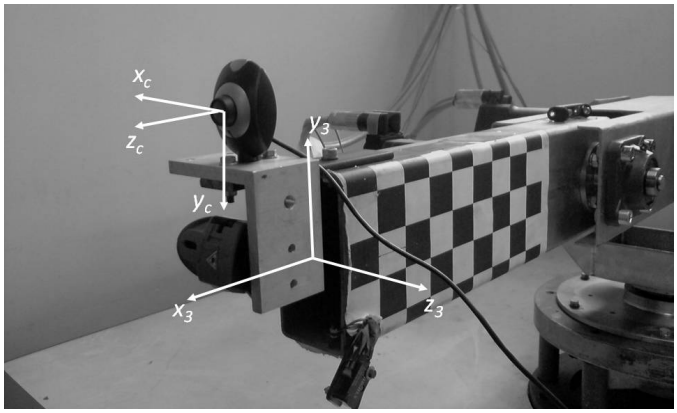

Fig. 32. Camera reference system.

By means of the equations (16), (17) and (29), the relationship between image coordinates (u,v) of the laser path and its coordinates in the robot base frame 0, is defined. By means of these equations, it is possible to reconstruct the 3D points in the robot base frame, of the intersection between the laser line and the object.
Robot positioning errors do not influence the 3D reconstruction, because each image is acquired and elaborated in a real robot position, that is known by means of robot encoders [12].

5.3 The data capture and the registration

The scanner video camera captures profiles from the surface of the object as 2D coordinates in the laser plane. During a scan sequence the laser scanner module is moved in order to capture object images from different sides and with different angles-shot according to the shape of the object.
In Matlab, an interactive GUI was developed in order to allows users to acquire and to elaborate data, figure 33. For each camera picture, along the scan path, the scanner derives a scan profile built up of point coordinates, in real-time.
The first step present in the GUI is the load of the calibration parameters that are composed by the laser scanner parameters and the matrix $[{}^{c}T_3]$. The second step is to filter the pixels of the laser path from the image, to do this, there are some regulations: the identification of the intensity of selected pixels, the calculus of the threshold and other regulations of the camera settings. The third step is to write the 3 joint position parameters of the robot in the window "position" , after this, clicking on the button "Image" the software save all the information, necessary for the reconstruction, in the workspace of the Matlab. Clicking on the button "3D generation" the software calculates the 3D positions of the laser path in the robot base frame, and the result is shown on the GUI window.

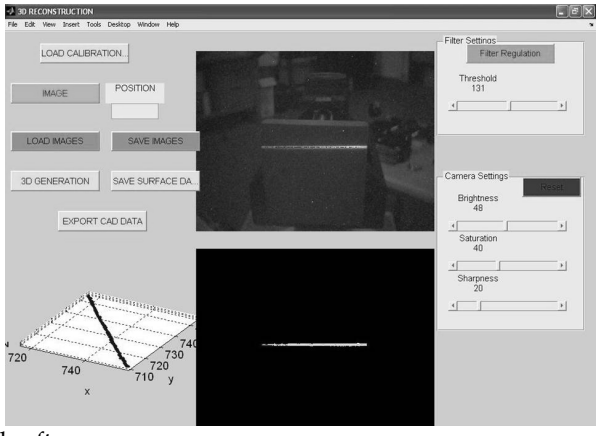

Fig. 33. Developed software.

When the scanning procedure is completed, the user can save images and relative robot position information in a file, save the cloud of points represent the surface of the test object and export the surface information in a file format that permits to load the data from the CAD software "CATIA".

Besides it's possible to load image information from a preview scanning procedure, this is useful for reconstruct the same laser path information using different calibration parameters.

5.4 The surfaces reconstruction

The system has been tested before in a fixed robot position, to verify calibration and reconstruction procedures, then the shape of some components, was defined using robot to move laser scanner module. The test objects are shown in the figure 34.

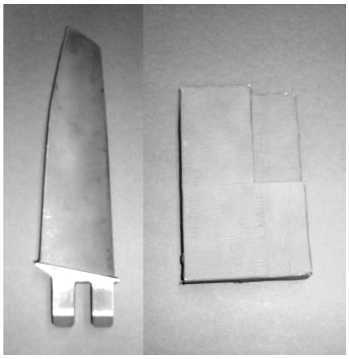

Fig. 34. Test specimens.

In the figure 35 and 36 it's possible to see a step of the procedure with the final results for the two test specimens.

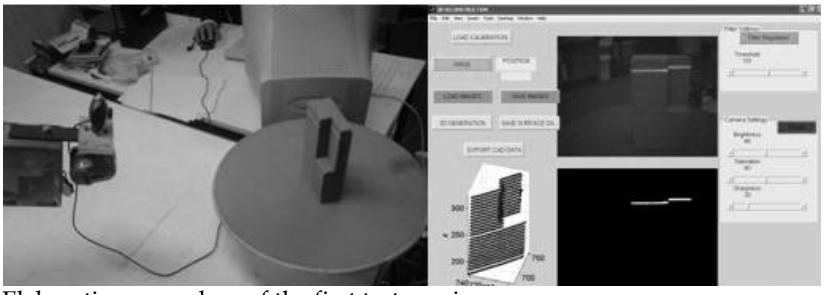

Fig. 35. Elaboration procedure of the first test specimen

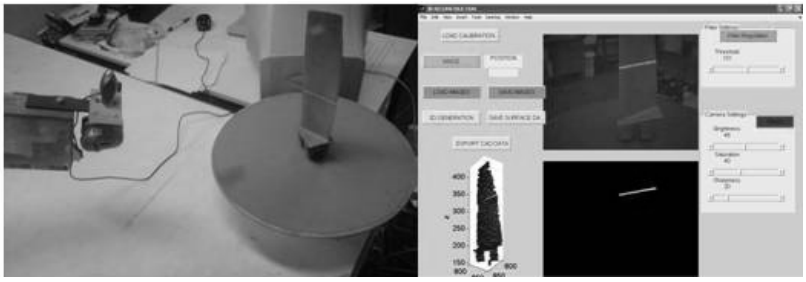

Fig. 36. Elaboration procedure of the second test specimen

By using the software CATIA it was possible to build the surface of the two test objects, in this way it was obtained the CAD model, this step of the 3D reconstruction method is a real reverse engineering application. The routine "Digitized shape editor" of the "CATIA" addresses digitalized data import, clean up, tessellation, cross sections, character line, shape and quality checking. In the figure 37 and 38 are shown the comparisons between the clouds of points and the respective surfaces for each object.

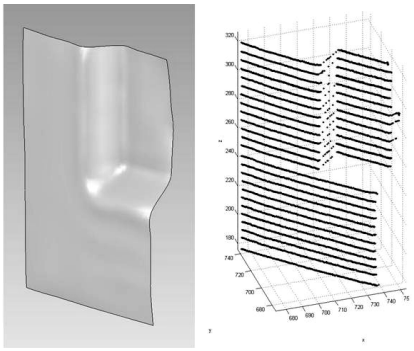

Fig. 37. First test specimen results

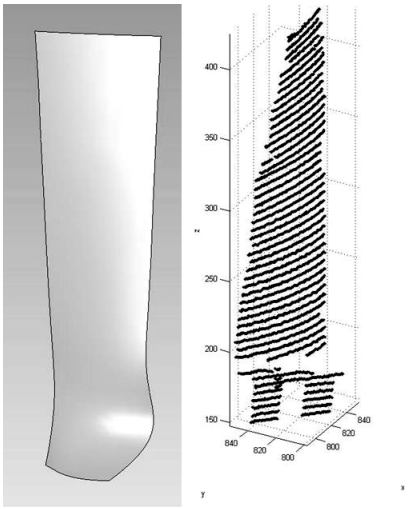

Fig. 38. Second test specimen results

In the figures 39 and 40, an evaluation of 3D-reconstruction accuracy is shown for the two analyzed test specimen. It is possible to observe, that these first results have the worst accuracy along direction z of camera frame, according to observations of paragraph 5.3.

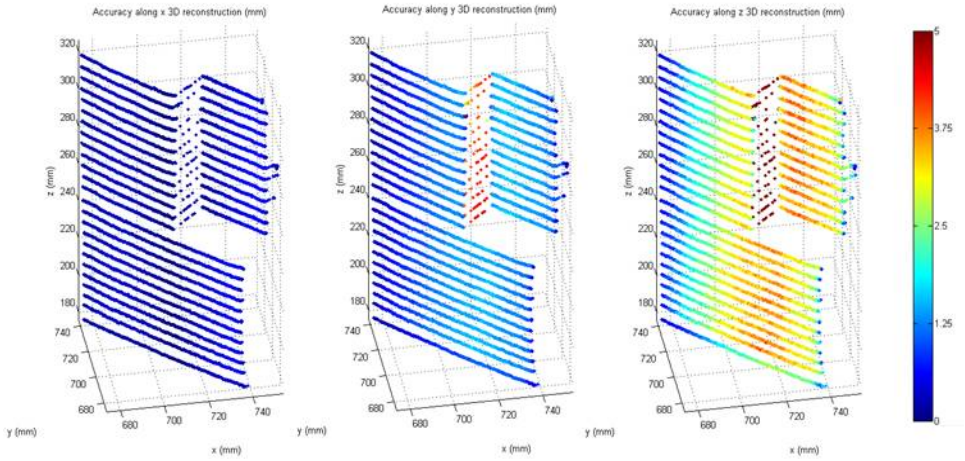

Fig. 39. First test specimen results

The results of the 3D reconstruction obtained by means of the rig that was designed and developed at authors' laboratory were compared with the ones obtained by means of a commercial 3D laser scanner. In the figures 41 and 42 the clouds of points obtained with the two different rigs are compared.

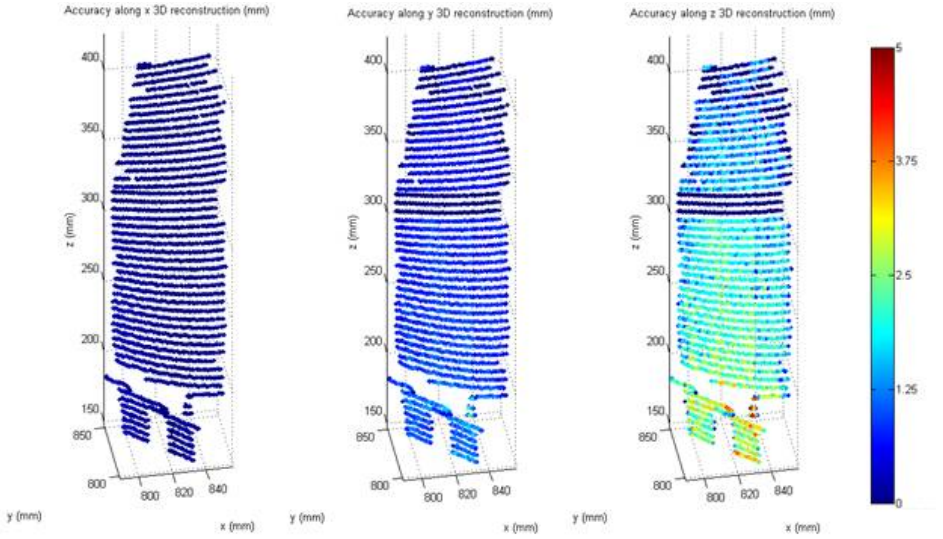

Fig. 40. Second test specimen results

Fig. 41. Cloud of points obtained by the aouthors' robot assisted rig.

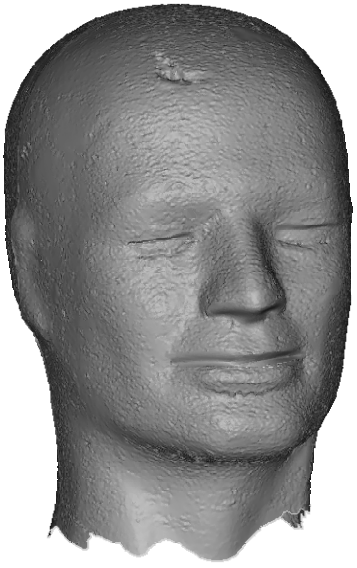

Fig. 42. Clouds of point obtained with commercial laser scanner.

In figure 43 is reported a comparison between the points obtained by the authors' rig and the commercial laser scanner. In figure 44 is reported a comparison between the surafces fobtaine by the above mentioned rigs.

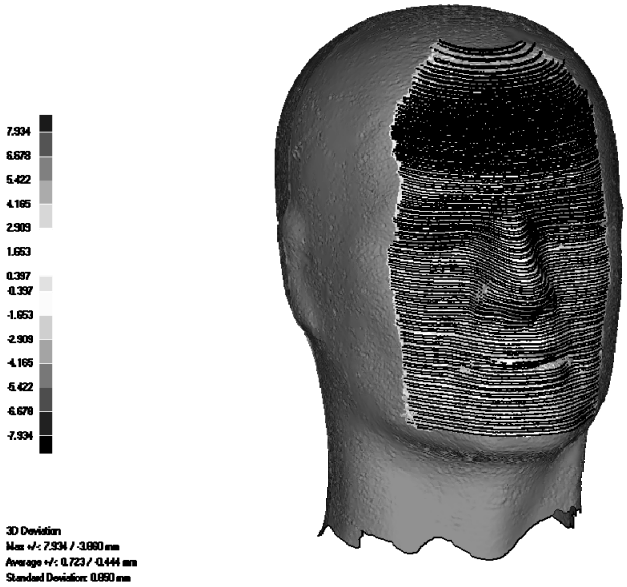

Fig. 43. Comparison between results obtained with two different rig.

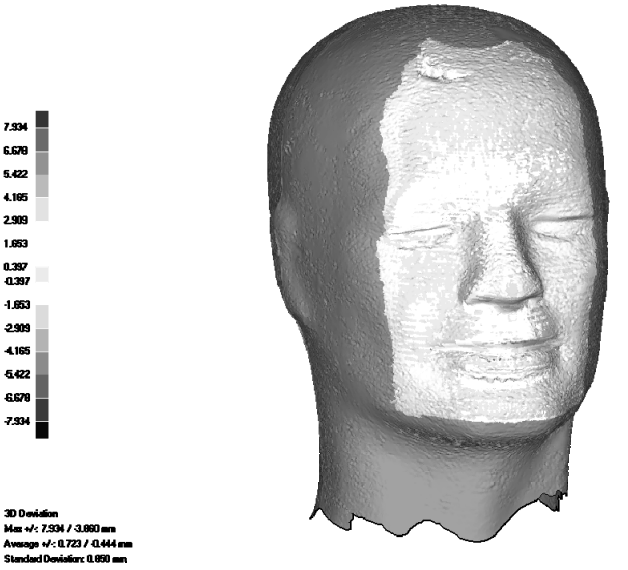

Fig. 44. Comparison between results obtained with two different rig.

It was observed that in most cases the differences are no more than ±1.5 mm; just in few areas the differences can reach 5 mm. A more detailed analisys showed that these differences concern single points, so it is possible to presume that a preliminary analisyss of the cloud of points could permit a general increase of the reconstruction accuracy.

6. Conclusions

The proposed procedures are absolutely non-invasive since they do not involve any modification of the scene; in fact no markers with features visible by both the camera and the laser, or any other device, are required.
As for the first results of the new method for real time shape acquisition by a laser scanner , it must be said that, although the test rig has been conceived just to validate the method (hence no high resolution cameras were adopted), the tests have showed encouraging results. These results can be summarized as follows.

1. It is possible to calibrate the intrinsic parameters of the video system, the position of the image plane and the laser plane in a given frame, all in the same time.
2. The surface shapes can be recognized and recorded with an appreciable accuracy.
3. The proposed method can be used for robotic applications such as robotic kinematic calibration and 3D surfaces recognition and recording. For this last purpose the test rig was fitted on a robot arm that permitted to the scanner device to 'observe' the 3D object from different and known position.

A detailed analysis of the sources of errors and the verification of the accuracy has been also carried on. As far as the latter aspect is concerned, the authors believe that a better system for tracking the position of the robot arm could enhance accuracy.
Finally, the authors would like to point out that the solution proposed is relatively low cost, scalable and flexible. It is also suitable for applications other than RE, like robot control or inspection.

7. References

[1] Fusiello, A. (2005). Visione Computazionale: appunti delle lezioni, *Informatic Department, University of Verona*, 3 March 2005.
[2] F. Blais (2004). Review of 20 years of range sensor development, *Journal of Electronic Imaging* , Vol. 13, No. 1, pp. 231–240.
[3] D. Acosta, O. García and J. Aponte (2006). Laser Triangulation for shape acquisition in a 3D Scanner Plus Scanner, *Proc. of the Electronics Robotics and Automotive Mechanics Conference*, 2006.
[4] J. Forest (2004). New methods for triangulation-based shape acquisition using laser scanners., *PhD thesis*, University of Girona, 2004.
[5] C. Colombo, D. Comanducci and A. Del Bimbo (2006). Low-Cost 3D Scanning by Exploiting Virtual Image Symmetries, *Journal of Multimedia*, Vol. 1, No. 7.
[6] N. Koller (2005). Fully Automated Repair of Surface Flaws using an Artificial Vision Guided Robotic Grinder, *PhD thesis*, University of Leoben, 2007.
[7] C. Matabosch (2007).Hand-held 3D-scanner for large surface registration, *PhD thesis*, University of Girona, 2007.
[8] M. Ritter, M. Hemmleb, O. Sinram, J. Albertz and H. Hohenberg (2004). A Versatile 3D Calibration Object for Various Micro-range Measurement Methods, *Proc. of ISPRS*, pp. 696-701, Istanbul, 2004.
[9] L.A. Albuquerque and J.M.S.T. Motta (2006). Implementation of 3D Shape Reconstruction from Range Images for Object Digital Modeling, *ABCM Symposium Series in Mechatronics*, Vol. 2, pp.81-88.

[10] Sören Larsson and J.A.P. Kjellander (2006). Motion control and data capturing for laser scanning with an industrial robot, *Robotics and Autonomous Systems*, Vol.54, No.6, pp. 453-460, 30 June 2006.

[11] R.A. Jarvis and Y.L. Chiu (1996). Robotic Replication of 3D Solids, *Proceedings of IROS*, 1996.

[12] V. Niola, C. Rossi and S. Savino (2007). Vision System for Industrial Robots Path Planning, *Journal of Mechanics and Control*.

[13] Cesare Rossi, Sergio Savino and Salvatore Strano (2008). 3D object reconstruction using a robot arm, *Proc. of 2-nd European Conference on Mechanism Science*, Cassino, Italy, 2008.

[14] J. Russell Noseworthy, Arthur M. Ryan, Lester A. Gerhardt (1991). Camera and Laser Scanner Calibration with Imprecise Data, *Proc. of Third Annual Conference on Intelligent Robotic Systems for Space Exploration*, pp. 99-111, 1991.

[15] C. Teutsch, T. Isenberg, E. Trostmann, M. Weber (2004). Evaluation and Optimization of Laser Scan Data, *15th Simulation and Visualisation*, March 4─5, 2004.